AD-A126 114 THEORY OF GYROTRON AMPLIFIER IN A TAPE HELIX LOADED WAVEGUIDE(U) NAVAL SURFACE WEAPONS CENTER SILVER SPRING MD H S UHM ET AL. SEP 82 NSWC/TR-82-528 1/1

UNCLASSIFIED SBI-AD-F500 142 F/G 9/1 NL

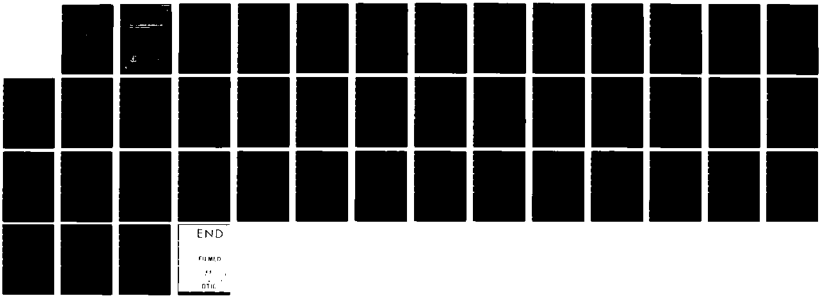

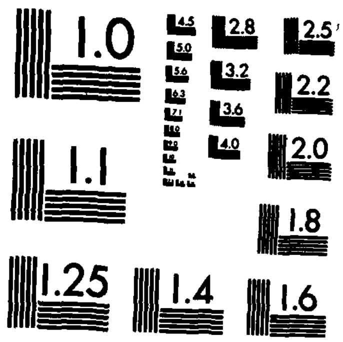

MICROCOPY RESOLUTION TEST CHART
NATIONAL BUREAU OF STANDARDS-1963-A

AD A126114

NSWC TR 82-[illegible]
PLASMA PHYSICS PUBLICATION NO. [illegible]

THEORY OF GYROTRON AMPLIFIER IN A TAPE HELIX LOADED WAVEGUIDE

BY HAN S. UHM,
JOON Y. CHOE

RESEARCH AND TECHNOLOGY DEPARTMENT

SEPTEMBER 1982

NAVAL SURFACE WEAPONS CENTER

Dahlgren, Virginia 22448 • Silver Spring, Maryland 20910

UNCLASSIFIED

SECURITY CLASSIFICATION OF THIS PAGE (When Data Entered)

REPORT DOCUMENTATION PAGE		READ INSTRUCTIONS BEFORE COMPLETING FORM
1. REPORT NUMBER NSWC TR 82-528	2. GOVT ACCESSION NO. AD-A126 114	3. RECIPIENT'S CATALOG NUMBER
4. TITLE (and Subtitle) THEORY OF GYROTRON AMPLIFIER IN A TAPE HELIX LOADED WAVEGUIDE		5. TYPE OF REPORT & PERIOD COVERED 6. PERFORMING ORG. REPORT NUMBER
7. AUTHOR(s) Han S. Uhm and Joon Y. Choe		8. CONTRACT OR GRANT NUMBER(s)
9. PERFORMING ORGANIZATION NAME AND ADDRESS Naval Surface Weapons Center (Code R41) White Oak Silver Spring, MD 20910		10. PROGRAM ELEMENT, PROJECT, TASK AREA & WORK UNIT NUMBERS 61152N; ZR00001; ZR01109; R01AA400
11. CONTROLLING OFFICE NAME AND ADDRESS		12. REPORT DATE September 1982 13. NUMBER OF PAGES 44
14. MONITORING AGENCY NAME & ADDRESS(if different from Controlling Office)		15. SECURITY CLASS. (of this report) UNCLASSIFIED 15a. DECLASSIFICATION/DOWNGRADING SCHEDULE

16. DISTRIBUTION STATEMENT (of this Report)

Approved for public release; distribution unlimited.

17. DISTRIBUTION STATEMENT (of the abstract entered in Block 20, if different from Report)

18. SUPPLEMENTARY NOTES

19. KEY WORDS (Continue on reverse side if necessary and identify by block number)

Gyrotron Amplifier
Helix Loaded Waveguide

20. ABSTRACT (Continue on reverse side if necessary and identify by block number)

Stability properties of the cyclotron maser instability in an annular electron beam propagating through a cylindrical waveguide loaded with a tape helix are investigated, in connection with applications on the gyrotron amplifier. Closed form of the dispersion relation for the cyclotron maser instability is obtained, including influence of the tape helix in stability behavior. It is shown that the bandwidth of the gyrotron amplifier for a tape helix is narrow in comparison with results for a sheath helix. However, the growth rate of the tape helix gyrotron is comparable to that of the sheath

DD FORM 1473, 1 JAN 73 EDITION OF 1 NOV 65 IS OBSOLETE
S/N 0102-LF-014-6601

UNCLASSIFIED

SECURITY CLASSIFICATION OF THIS PAGE (When Data Entered)

helix gyrotron.

FOREWORD

Stability properties of the cyclotron maser instability in an annular electron beam propagating through a cylindrical waveguide loaded with a tape helix are investigated, in connection with applications on the gyrotron amplifier. Closed form of the dispersion relation for the cyclotron maser instability is obtained, including influence of the tape helix in stability behavior. It is shown that the bandwidth of the gyrotron amplifier for a tape helix is narrow in comparison with results for a sheath helix. However, the growth rate of the tape helix gyrotron is comparable to that of the sheath helix gyrotron.

Approved by:

Ira M Blatstein

IRA M. BLATSTEIN, Head
Radiation Division

CONTENTS

ILLUSTRATIONS

I. INTRODUCTION

In recent years, stability properties of the electron cyclotron maser instability[1-4] have been investigated in a great detail, in connection with applications on the gyrotron amplifiers. Particularly, motivated by a wide bandwidth microwave amplification, properties of the gyrotron amplifier in a sheath helix loaded waveguide have been also investigated in a previous study.[5] Although a theoretical analysis in a sheath helix loaded waveguide is a reasonable simplifying assumption in many experiments, we expect a significant modification of the stability behavior when the sheath helix is replaced by a more practical tape helix. In this regard, this paper examines properties of the cyclotron maser instability in a hollow electron beam propagating through a tape helix loaded waveguide.

This paper extends the previous theory of the cyclotron maser instability, developed by the authors for a sheath helix loaded waveguide, to a tape helix loaded waveguide. The analysis is carried out within the framework of the Vlasov-Maxwell equations for an infinitely long hollow electron beam with radius R_0, propagating parallel to a uniform magnetic field $B_0 \hat{\mathbf{e}}_z$ with axial velocity $\beta_z c \hat{\mathbf{e}}_z$. The radii of the helix and the grounded conducting wall are denoted by R_h and R_c, respectively. Equilibrium and stability properties are calculated for the electron distribution function [Equation (3)] in which all electrons have the same energy and the same canonical angular momentum but a Lorentzian distribution in the axial canonical momentum. We assume that the hollow beam is thin and very tenuous. The formal dispersion relation [Equation (31)] of the cyclotron maser instability is obtained in Section IV, including the important influence of the presence of a tape helix.

In Section IV, properties of the vacuum waveguide mode loaded with a tape helix are briefly investigated without including the influence of beam electrons. Stability properties of the cyclotron maser instability are numerically investigated in Section IV, in connection with application on the gyrotron amplifier. It is shown that the bandwidth of the tape helix gyrotron amplifier for a helix mode is narrow in comparison with results of the sheath helix gyrotron amplifier. However, the growth rate of the tape helix gyrotron is comparable to that of the sheath helix gyrotron. In addition, the growth rate and bandwidth of the gyrotron amplifier for tape helix are relatively less effected by the axial momentum spread than those for sheath helix.

II. LINEARIZED VLASOV-MAXWELL EQUATIONS FOR PERTURBATION

The equilibrium configuration consists of a relativistic annular electron beam propagating parallel to a strong, externally applied magnetic field $B_0\hat{\underset{\sim}{e}}_z$. The mean radius of the electron beam is denoted by R_0, and a grounded cylindrical conducting wall is located at radius $r = R_c$. Cylindrical polar coordinates (r,θ,z) are introduced in the analysis. A helix tape with width δ and zero thickness is located between the electron beam and conducting wall. The radius and pitch of the helix are denoted by R_h and L, respectively, thereby defining the pitch angle ϕ and the unit helix vector $\hat{\underset{\sim}{e}}_\phi$ by

$$\cot\phi = 2\pi R_h/L \tag{1}$$

and

$$\hat{\underset{\sim}{e}}_\phi = \cos\phi\ \hat{\underset{\sim}{e}}_\theta + \sin\phi\ \hat{\underset{\sim}{e}}_z \tag{2}$$

where $\hat{\underset{\sim}{e}}_\theta$ and $\hat{\underset{\sim}{e}}_z$ are unit vectors on the azimuthal and axial directions. Obviously, it is assumed $R_0 < R_h < R_c$.

In the analysis, we also assume that $\nu/\hat{\gamma} << 1$, where $\nu = N_b e^2/mc^2$ is Budker's parameter and $\hat{\gamma}mc^2$ is the electron energy. Here N_b is the total number of electrons per unit axial length, -e and m are the charge and rest mass of electrons, respectively. Moreover, it is further assumed that the electron beam is thin, i.e., $(R_2-R_1) << R_0$, where R_1 and R_2 are the inner

and outer radii, respectively, of the annular electron beam. In the present analysis, we investigate stability properties for the choice of equilibrium distribution function

$$f_b^0\,(H,\,P_\theta,P_z) = \frac{\hat{\omega}_c N_b \hat{p}_z \Delta}{4\pi^3 \hat{\gamma} mc^2}\;\frac{\delta(\gamma-\hat{\gamma})\;\delta\,(P_\theta - P_0)}{(p_z-\hat{p}_z)^2 + \hat{p}_z^{\,2}\Delta^2}, \tag{3}$$

Where $H = \gamma mc^2 = (m^2c^4 + c^2p^2)^{1/2}$ is the total energy, p_z is the axial momentum, $P_\theta = r\left[p_\theta - (e/2c)rB_0\right]$ is the canonical angular momentum, $\hat{\omega}_c = eB_0/mc$ is the non-relativistic electron cyclotron frequency, $P_0 = -(e/2c)\,(R_0^2 - r_L^2)\,B_0$ is the canonical angular momentum of an electron with Larmor radius $r_L = \left[(\gamma^2 - 1)\,c^2/\hat{\omega}_c^2 - (p_z/m\hat{\omega}_c)^2\right]^{1/2}$, and $\hat{\gamma}$, $\hat{p}_z$ and Δ are constants.

Making use of Floquet's theorem,[6, 7] we adopt a normal mode approach in which all perturbations are assumed to vary according to

$$\psi(\underset{\sim}{x},t) = \sum_{n=-\infty}^{\infty} \hat{\psi}_n(r)\exp\{i(n\theta + k_n z - \omega t)\} \tag{4}$$

where

$$k_n = k - 2\pi(n-\ell)/L \tag{5}$$

is the axial wavenumber of the component n, ω and k are the oscillation frequency and the axial wavenumber, respectively, and ℓ represents the primary azimuthal mode number. For example, for small k value, the electromagnetic field for $n = \ell$ azimuthal harmonic perturbation is dominant.[6]

In the present purposes, it is assumed that

$$|\omega - \hat{\omega}_c/\hat{\gamma} - (k + 2\pi s/L)\beta_z c| << \hat{\omega}_c/\hat{\gamma},\ 2\pi\beta_z c/L \tag{6}$$

where $\beta_z = \hat{p}_z/\hat{\gamma}mc$, c is the speed of light in vacuo, and s is the space harmonic number. The Maxwell equations for the perturbed electric and magnetic field amplitudes can be expressed as

$$\begin{aligned} \nabla \times \hat{E}(x) &= i(\omega/c)\,\hat{B}(x) \\ \nabla \times \hat{B}(x) &= (4\pi/c)\,\hat{J}(x) - i\,(\omega/c)\,\hat{E}(x), \end{aligned} \tag{7}$$

where $\hat{E}(x)$ and $\hat{B}(x)$ are the perturbed electric and magnetic fields and $\hat{J}(x)$ is the perturbed current density.

Within the content of a thin beam approximation and Eq. (6), the transverse components of the perturbed current density in Eq. (4) is expressed as[5]

$$\begin{aligned} \hat{J}_\theta(x) = i\hat{J}_r(x) &= \frac{c}{4\pi} \exp\{i(\alpha\theta + k_\alpha z)\} \\ &\times \left[\hat{E}_{\theta\alpha}(R_0) + i\,\hat{E}_{r\alpha}(R_0)\right] \chi(\omega,k)\ \delta\,(r - R_0) \end{aligned} \tag{8}$$

where the effective susceptibility $\chi(\omega,k)$ is defined by

$$\chi(\omega,k) = -\,i\,\frac{\nu\beta_\perp^2 c}{2\hat{\gamma}\omega R_0}\,\frac{\omega^2 - k_\alpha^2 c^2}{(\Omega + i|k_\alpha|\beta_z c\hat{\gamma}\Delta/\gamma_z^3)^2}, \tag{9}$$

$$\Omega = \omega - k_\alpha \beta_z c - \hat{\omega}_c/\hat{\gamma} \tag{10}$$

is the Doppler-shifted eigenfrequency, $\beta_\perp = p_\perp/\hat{\gamma}mc$, $\beta_z = \hat{p}_z/\hat{\gamma}mc = (\gamma_z^2 - 1)^{1/2}/\gamma_z$,

$\nu = N_b e^2/mc^2$ is the Budker's parameter and the integer α is defined by

$$\alpha = \ell - s. \tag{11}$$

As noted from Eq. (8), we emphasize that consistent with Eq. (6), the transverse current density is mainly originated from perturbations with $n = \alpha$ since the corrections associated with other perturbations with $n \neq \alpha$ are order $\Omega L/2\pi\beta_z c$ $(\ll 1)$ or smaller.[5] Moreover, we can also approximate the perturbed charge and the axial component of the perturbed current density by

$$\hat{\rho}(r) = \hat{J}_z(r) = 0.$$

In this regard, from the Maxwell equation (7), we obtain

$$\left\{\frac{1}{r}\frac{\partial}{\partial r} r \frac{\partial}{\partial r} - \frac{n^2}{r^2} + \frac{\omega^2}{c^2} - k_n^2\right\}\hat{E}_{zn}(r) = 0 \tag{12}$$

for the axial component of the electric field with arbitrary n. Similarly, for the axial component of the magnetic field, the Maxwell equation (7) is expressed as

$$\left\{\frac{1}{r}\frac{\partial}{\partial r} r \frac{\partial}{\partial r} - \frac{n^2}{r^2} + \frac{\omega^2}{c^2} - k_n^2\right\}\hat{B}_{zn}(r) = 0 \tag{13}$$

for $n \neq \alpha$ and

$$\left\{\frac{1}{r}\frac{\partial}{\partial r} r \frac{\partial}{\partial r} - \frac{\alpha^2}{r^2} + \frac{\omega^2}{c^2} - k_\alpha^2\right\}\hat{B}_{z\alpha}(r)$$

$$= -\frac{4\pi}{c}\left\{\frac{1}{r}\frac{\partial}{\partial r}\left[r\hat{J}_{\theta\alpha}(r)\right] - i\frac{\alpha}{r}\hat{J}_{r\alpha}(r)\right\}, \tag{14}$$

where the r- and θ- components of the perburbed current density $\hat{J}_{r\alpha}(r)$ and $\hat{J}_{\theta\alpha}(r)$ are defined in Eq. (8)

The physically acceptable solution to Eq. (12) is

$$\hat{E}_{zn}(r) = a_n \begin{cases} J_n(p_n r), \quad 0 \leq r \leq R_h, \\ J_n(\eta_n) \dfrac{N_n(\zeta_n)J_n(p_n r) - J_n(\zeta_n)N_n(p_n r)}{J_n(\eta_n)N_n(\zeta_n) - J_n(\zeta_n)N_n(\eta_n)}, \\ \qquad R_h \leq r \leq R_c, \end{cases} \tag{15}$$

for all n. However, for the axial component of the magnetic field, we have

$$\hat{B}_{zn}(r) = \begin{cases} b_\alpha\left[J_\alpha(p_\alpha r) + g\,(\omega,k)N_\alpha(p_\alpha r)\right], \; n = \alpha, \\ b_n\; J_n(p_n r), \; n \neq \alpha, \end{cases} \tag{16}$$

for $R_0 < r < R_h$, and

$$\hat{B}_{zn}(r) = b_n J_n'(\eta_n) \frac{N_n'(\zeta_n) J_n(p_n r) - J_n'(\zeta_n) N_n(P_n r)}{J_n'(\eta_n) N_n'(\zeta_n) - J_n'(\zeta_n) N_n'(\eta_n)}, \tag{17}$$

for $R_n < r \leq R_c$ and for all n. In Eqs. (15) - (17), a_n and b_n are constants. $J_n(x)$ and $N_n(x)$ are the Bessel functions of the first and second kinds, respectively, of order n, the prime (') denotes (d/dx) $J_n(x)$ and (d/dx) $N_n(x)$, and the parameters η_n, ζ_n and p_n are defined by

$$\eta_n^2 = \zeta_n^2 R_h^2/R_c^2 = p_n^2 R_h^2 = (\omega^2/c^2 - k_n^2) R_h^2. \tag{18}$$

The boundary conditions of the magnatic field at $r = R_h$ for the tape helix are[6, 7]

$$\hat{B}_z^i - \hat{B}_z^o = \frac{4\pi}{c} \hat{J}_\parallel \cos\phi,$$
$$\hat{B}_\theta^o - \hat{B}_\theta^i = \frac{4\pi}{c} \hat{J}_\parallel \sin\phi, \tag{19}$$

where the superscript i and o represent the magnetic field components at just inside and just outside, respectively, of the helix tape, $\hat{J}_\parallel$ is the surface current density along the helix direction with the unit vector $\hat{e}_\phi$. Assuming that the current in the tape flows only in the tape direction, and that it does not vary in phase or amplitude over the width of the tape, the surface current

density $\hat{J}_{\parallel}$ is reasonably expressed as[6, 7]

$$\hat{J}_{\parallel} = \sum_n j_{\parallel n} \exp\{i(n\theta + k_n z)\} \tag{20}$$

where the component amplitude $j_{\parallel n}$

$$j_{\parallel n} = \hat{J} \exp(-ik_n\delta/2) \frac{\sin(k_n\delta/2)}{k_n\delta/2} \tag{21}$$

and δ is the width of the helix tape. Substituting Eqs. (15) - (17) and (20) into Eq. (19), it is straightforward to show that

$$a_n = -i\frac{p_n}{\omega}2\pi^2 j_{\parallel n}\eta_n \cos\phi\left(\tan\phi - \frac{k_n n}{\eta_n p_n}\right)$$

$$\times \frac{J_n(\zeta_n)N_n(\eta_n) - J_n(\eta_n)N_n(\zeta_n)}{J_n(\zeta_n)} \tag{22}$$

and

$$b_n = \frac{2\pi^2}{c} j_{\parallel n} \cos\phi\, \eta_n \left[J_n'(\zeta_n)N_n'(\eta_n) - J_n'(\eta_n)N_n'(\zeta_n)\right]$$

$$\times \begin{cases} \left[J_\alpha'(\zeta_\alpha) + gN_\alpha'(\zeta_\alpha)\right]^{-1}, & n = \alpha, \\ \left[J_n'(\zeta_n)\right]^{-1}, & n \neq \alpha. \end{cases} \tag{23}$$

At the helix surface, the electric field along the helix direction is given by

$$\hat{E}_{\parallel}(\underset{\sim}{x}) = \sum_n \exp\{i(n\theta + k_n z)\}\left[\hat{E}_{\theta n}(R_h)\cos\phi + \hat{E}_{zn}(R_h)\sin\phi\right]. \tag{24}$$

Making use of the Maxwell equation (7), and Eqs. (15) and (16), we can show that Eq. (24) is expressed as

$$\hat{E}_{\parallel}(\underset{\sim}{x}) = \cos\phi \sum_n \exp\{i(n\theta + k_n z)\}$$

$$\times \left\{ a_n J_n(\eta_n)\left(\tan\phi - \frac{k_n n}{\eta_n p_n}\right) - i\frac{\omega}{cp_n} b_n\left[J_n'(\eta_n) + g_n N_n'(\eta_n)\right]\right\}, \tag{25}$$

where $g_n = g$ for $n = \alpha$ and $g_n = 0$ otherwise. The coefficient function $g(\omega,k)$ in Eq. (25) can be expressed in terms of the helix and geometric parameters, assuming that the electric field in Eq. (25) is set equal to zero along the center line of the tape, i.e., at $z = (L\theta/2\pi) + (\delta/2)$. This assumption is a good approximation for narrow tapes. Substituting Eqs. (22) and (23) into Eq. (25), and carrying out a tedius but straightforward algebra, we obtain

$$g(\omega,k) = -\frac{J_\alpha'(\zeta_\alpha)}{N_\alpha'(\zeta_\alpha)}\,\frac{D(\omega,k)}{F(\omega,k)} \tag{26}$$

where the vacuum dispersion function $D(\omega,k)$ is defined by [7]

$$D(\omega,k) = \sum_n \frac{\sin(k_n\delta/2)}{k_n\delta/2}\left\{\eta_n^2\left(\tan\phi - \frac{k_n n}{\eta_n p_n}\right)^2 \frac{J_n(\eta_n)}{J_n(\zeta_n)}\right.$$

$$\times\left[J_n(\zeta_n)N_n(\eta_n) - J_n(\eta_n)N_n(\zeta_n)\right]$$

$$\left. + \frac{\omega^2 R_h^2}{c^2}\frac{J_n'(\eta_n)}{J_n'(\zeta_n)}\left[J_n'(\zeta_n)N_n'(\eta_n) - J_n'(\eta_n)N_n'(\zeta_n)\right]\right\} \tag{27}$$

and the function $F(\omega,k)$ is given by

$$F(\omega,k) = D(\omega,k) + \frac{\omega^2 R_h^2}{c^2}\frac{\sin(k_\alpha\delta/2)}{k_\alpha\delta/2}$$

$$\times\frac{\left[J_\alpha'(\zeta_\alpha)N_\alpha'(\eta_\alpha) - J_\alpha'(\eta_\alpha)N_\alpha'(\zeta_\alpha)\right]^2}{J_\alpha'(\zeta_\alpha)N_\alpha'(\zeta_\alpha)}, \tag{28}$$

where $k_n = k - 2\pi(n-\ell)/L$ defined in Eq. (5), and the parameters, η_n, ζ_n and p_n are given in Eq. (18).

Evidently from Eqs. (13) and (14), the axial component of the perturbed magnetic field is continuous across $r = R_0$ for all n ·· cept $n = \alpha$. For $n = \alpha$, the physically acceptable solution to Eq. (14) is given by

$$\hat{B}_{z\alpha}(r) = \begin{cases} b_{in}\, J_\alpha(p_\alpha r), & 0 \le r < R_0, \\ b_\alpha\left[J_\alpha(p_\alpha r) + gN_\alpha(p_\alpha r)\right], & R_0 < r < R_h, \end{cases} \tag{29}$$

where b_{in} and b_α are constants. For convenience in the subsequent analysis, we introduce the normalized magnetic wave admittance $b_\pm$ defined at the inner and outer surfaces of the electron beam by

$$b_+ = -\hat{B}_{z\alpha}(R_0^+)/[r(\partial/\partial r)\hat{B}_{z\alpha}]_{R_0^+}$$

$$b_- = \hat{B}_{z\alpha}(R_0^+)/[r(\partial/\partial r)\hat{B}_{z\alpha}]_{R_0^-}. \qquad (30)$$

Making use of Eqs. (7), (8) and (30), we obtain the dispersion relation of the gyrotron amplifier in a tape helix waveguide

$$\Gamma(\omega,k) = -\frac{\nu\beta_\perp^2 c^2}{2\hat{\gamma}\, R_0^2(\Omega+i|k_\alpha|\beta_z c\hat{\gamma}\Delta/\gamma_z^3)^2}, \qquad (31)$$

where the admittance function $\Gamma(\omega,k)$ is defined by

$$\Gamma(\omega,k) = \frac{2g(\omega,k)/\pi\xi_\alpha^2 J_{\alpha-1}^2(\xi_\alpha)}{1 + G(\omega,k)}, \qquad (32)$$

$$G(\omega,k) = g\,\frac{N_{\alpha-1}(\xi_\alpha)}{J_{\alpha-1}(\xi_\alpha)} + \frac{k_\alpha/p_\alpha}{\tan\phi - k_\alpha\alpha/p_\alpha^2 R_h}\;\frac{J_\alpha'(\eta_\alpha) + gN_\alpha'(\eta_\alpha)}{J_\alpha(\eta_\alpha)} \qquad (33)$$

and the parameter ξ_α is defined by

$$\xi_\alpha^2 = \zeta_\alpha^2 R_0^2/R_c^2 = (\omega^2/c^2 - k_\alpha^2)R_0^2 \qquad (34)$$

The dispersion relation in Eq. (31), combined with Eqs. (32) and (33), is one of the main results of this paper and can be used to investigate gain and bandwidth of the gyrotron amplifier for a broad range of physical parameters.

III. VACUUM WAVEGUIDE MODES

Assuming no beam electrons ($\nu \to 0$) in this section, we obtain the vacuum dispursion relation

$$D\ (\omega,k) = 0 \tag{35}$$

from Eqs. (26), (31) and (32). In Eq. (35), the vacuum dispersion function $D\ (\omega,k)$ is defined in Eq. (27). Even though the dispersion relation is a very complicated transcendental function of ω and k, in the limiting case where the outer conducting wall is very close to the helix (i.e., $R_c/R_h \to 1$), the vacuum dispersion relation is simplified to three distintive relations.[7] These are the transverse electric like, the transverse magnetic like and the helix modes. Particularly, the helix mode is represented by a straight line

$$\omega = \pm\left[\, kc \sin\phi + \ell\ (c/R_c)\ \cos\phi \right] \tag{36}$$

in the (ω,k) parameter space. The characteristic electron beam mode in the gyrotron amplifier is given by

$$\omega = k\beta_z c + (2\pi s/L)\beta_z c + \hat{\omega}_c/\hat{\gamma} \tag{37}$$

from Eq. (6). In this regard, we conclude from Eqs. (36) and (37) that a super wideband microwave amplifier can be developed by a choice of beam parameters satisfying

$$\beta_z \simeq \sin\phi,$$

$$\hat{\omega}_c/\hat{\gamma} = (c/R_c)\cos\phi\ (\ell - s), \tag{38}$$

for $R_c/R_h \simeq 1$.

In general case where $R_c/R_h \neq 1$, the dispersion relation in Eq. (35) is numerically solved to find ω for specified k value. Shown in Fig. 1 is plots of the normalized oscillation frequency $\omega R_h/c \cos\phi$ versus the normalized axial wave number $kR_h \tan\phi$ for $\ell = 0$ helix mode, $\phi = \pi/6$, $\delta/L = 0.3$ and several values of the parameter R_c/R_h. It is noted from Fig. 1 that dispersion curves of the helix mode approach to the straight line defined by Eq. (36) as the parameter R_c/R_h is reduced to unity. Moreover, the helix mode dispersion curves wiggle more prominately as the parameter R_c/R_h increases from unity to infinity. Obviously in the limit $R_c/R_h \to \infty$, every minimum points of ω in the dispersion curves are equal to zero. Detailed analytic and numerical investigation of the dispersion relation in Eq. (27) and (35) has been carried out in the previous literature [7] by authers. For additional information of the vacuum dispersion properties, we urge the reader to review this literature.[7]

IV. CYCLOTRON MASER INSTABILITY

In this section, we investigate stability properties of the cyclotron maser instability in a hollow electron beam propagating through a tape helix loaded waveguide, by making use of the dispersion relation in Equation (31). The growth rate and bandwidth of the cyclotron maser instability are directly related to the gain and bandwidth of the tape helix gyrotron amplifier. Making use of the fact that the "Doppler-shifted" eigenfrequency in Equation (10) is well removed from the electron cyclotron resonance, i.e., $|\Omega| << \hat{\omega}_c/\hat{\gamma}$ and evaluating the wave admittance function $\Gamma(\omega, k)$ at $k = k_b = (\omega - \hat{\omega}_c/\hat{\gamma})/\beta_z c - 2\pi s/L$, the dispersion relation in Equation (31) can be approximated by

$$\left[\Gamma(\omega, k_b) - \frac{1}{\beta_z c}\left(\frac{\partial}{\partial k}\Gamma\right)_{k_b}\Omega\right]\left[\Omega + i\,\frac{|\omega - \hat{\omega}_c/\hat{\gamma}|\hat{\gamma}\Delta}{\gamma_z^3}\right]^2$$

$$\simeq -\frac{\nu\beta_\perp{}^2c^2}{2\hat{\gamma}\,R_0{}^2}\ . \tag{39}$$

In the remainder of this section, the growth rate $\Omega_i = \mathrm{Im}\Omega$ and the Doppler-shifted real oscillation frequency $\Omega_r = \mathrm{Re}\Omega$ are numerically calculated from Equation (39) for the electron beam parameters $\nu = 0.002$, $\beta_\perp = 0.4$ and $\hat{\gamma} = 1.118$ ($\beta_z = 0.2$). Obviously from Equation (10), the normalized gain $k_i c/\hat{\omega}_c$ is expressed as

$$k_i c/\hat{\omega}_c = -\Omega_i/\beta_z. \tag{40}$$

Shown in Figure 2 is plots of the normalized growth rate $k_i c/\hat{\omega}_c$ versus $\omega/\hat{\omega}_c$ obtained from Equation (39) for the helix mode, $R_c/R_h = 1.1$, $R_0 = R_h - r_L$, $s = 0$,

$\delta/L = 0.3$, (a) $\Delta = 0.02$ and (b) $\Delta = 0.04$, and optinum values of the parameters $(R_h\hat{\omega}_c/c,\ \phi)$ for each azimuthal harmonic number ℓ. The optimum values of the parameter $(R_h\hat{\omega}_c/c,\ \phi)$ are given by (1.06, 10.7°) for $\ell = 1$, (2.15, 11.4°) for $\ell = 2$, (3.2, 11°) for $\ell = 3$ and (4.2, 10°) for $\ell = 4$. The bandwidth of the tape helix gyrotron amplifier for the helix mode in Figure 2 is narrow in comparison with results of the sheath helix gyrotron amplifier.[5] However, the growth rate of the tape helix gyrotron for the helix mode is comparable to that of the sheath helix gyrotron. In addition, the growth rate and bandwidth in Figure 2 are relatively less effected by the axial momentum spread Δ than those of the sheath helix gyrotron.

In general, we can show[5]

$$\Gamma(\omega,\ k_b) \simeq 0,$$
$$[\partial\Gamma(\omega,\ k)/\partial k]_{k_b} \simeq 0, \tag{41}$$

near the minimum oscillation frequency ω_0 in the hybrid vacuum waveguide mode and its corresponding wavenumber k_0. Therefore, in order to correctly evaluate the gain of the gyrotron amplifier at $(\omega,\ k) = (\omega_0,\ k_0)$, we approximate Equation (31) by

$$\left[\Gamma(\omega,\ k_b) - \frac{1}{\beta_z c}\left(\frac{\partial}{\partial k}\Gamma\right)_{k_b}\Omega + \frac{1}{2\beta_z^2\ c^2}\left(\frac{\partial^2}{\partial k^2}\Gamma\right)_{k_b}\Omega^2\right]$$
$$\times\ \left[\Omega + i\,\frac{|\omega - \hat{\omega}_c/\hat{\gamma}|\hat{\gamma}\Delta}{\gamma_z^3}\right]^2 = -\frac{\nu\beta_\perp{}^2c^2}{2\hat{\gamma}\ R_0{}^2} \tag{42}$$

Of course, the dispersion relation in Equation (39) is used to obtain the gain for a broad range of physical parameters except near the point $(\omega, k) = (\omega_0, k_0)$ where use of Equation (42) is made to estimate the gain.

As a typical example of the gyrotron amplifier for the hybrid waves, which consist of the transverse electric and transverse magnetic modes, shown in Figure 3 are plots of the normalized gain $k_i c/\hat{\omega}_c$ versus $\omega/\hat{\omega}_c$ obtained from Equations (39) and (42) for $s = 0$, $R_c/R_h = 1.5$, $\delta/L = 0.3$, $\Delta = 0.04$, $R_0 = R_h - r_L$, $\phi = -30°$ and $R_h\hat{\omega}_c/c = 1.86$ for $\ell = 0$, $R_h\hat{\omega}_c/c = 1.45$ for $\ell = 1$ and $R_h\hat{\omega}_c/c = 2.4$ for $\ell = 2$. The maximum gain in Figure 3 is considerably larger than that of the ordinary gyrotron amplifier. For example, the maximum growth rate for the $\ell = 1$ prturbation in Figure 3 is more than triple that of a smooth conducting waveguide without helix. As expected, the bandwidth of the tape helix gyrotron is narrower than that of the sheath helix gyrotron.[5]

In order to illustrate influence of the space harmonic number s on stability behavior, Figure 4 presents plots of the normalized growth rate versus $\omega/\hat{\omega}_c$ obtained from Equations (39) and (42) for $\ell = 2$, $R_c/R_h = 1.5$, $\delta/L = 0.3$, $\phi = -30°$, and (a) $s = 1$ and corresponding optimum value $R_h\hat{\omega}_c/c = 2.15$, (b) $s = 0$ and $R_h\hat{\omega}_c/c = 2.4$ and (c) $s = -1$ and $R_h\hat{\omega}_c/c - 2.54$. As expected from the relation

$$\omega/\hat{\omega}_c \simeq [1 + (c/R_h\hat{\omega}_c)\beta_z\hat{\gamma}\ s \cot \phi]/\hat{\gamma}, \tag{43}$$

the eigenfrequency correspnnding to the maximum growth rate increases with decreasing value of the space harmonic number s for a negative pitch angle. However, the gain reduces drastically when the eigenfrequency of the maximum growth rate increases.

V. CONCLUSIONS

In this paper, we have examined the excitation of electromagnetic waveguide modes by the cyclotron maser instability in a hollow electron beam propagating through a waveguide loaded with a tape helix. Stability analysis was carried out within the framework of the linearized Vlasov-Maxwell equations, assuming that the electron beam is thin and tenuous. The formal dispersion relation of the cyclotron maser instability was obtained in Section II, including the important influence of the presence of a tape helix. Properties of the vacuum waveguide mode loaded with a tape helix were briefly investigated in Section III, without including the influence of beam electrons. Stability properties of the cyclotron maser instability were numerically investigated in Section IV, in connection with application on the gyrotron amplifier. It was shown that the bandwidth of the tape helix gyrotron amplifier for a helix mode is narrow in comparison with results of the sheath helix gyrotron amplifier. However, the growth rate of the tape helix gyrotron is comparable to that of the sheath helix gyrotron.

VI. ACKNOWLEDGEMENTS

It is a pleasure to acknowledge the useful numerical calculations carried out by Miss Chung M. Kim.

This research was supported by the Independent Research Fund at the Naval Surface Weapons Center.

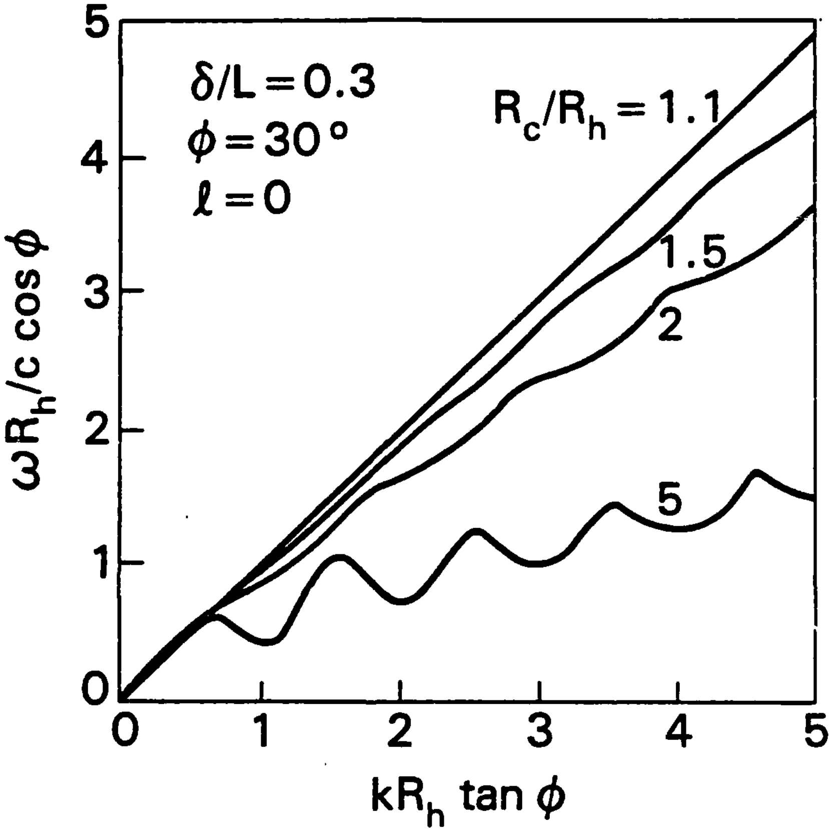

FIGURE 1. PLOTS OF THE NORMALIZED OSCILLATION FREQUENCY $\omega R_h/c\cos\phi$ VERSUS THE NORMALIZED AXIAL WAVE NUMBER $kR_h\tan\phi$ FOR $\ell = 0$ HELIX MODE, $\phi = \pi/6$, $\delta/L = 0.3$ AND SEVERAL VALUES OF THE PARAMETER R_c/R_h

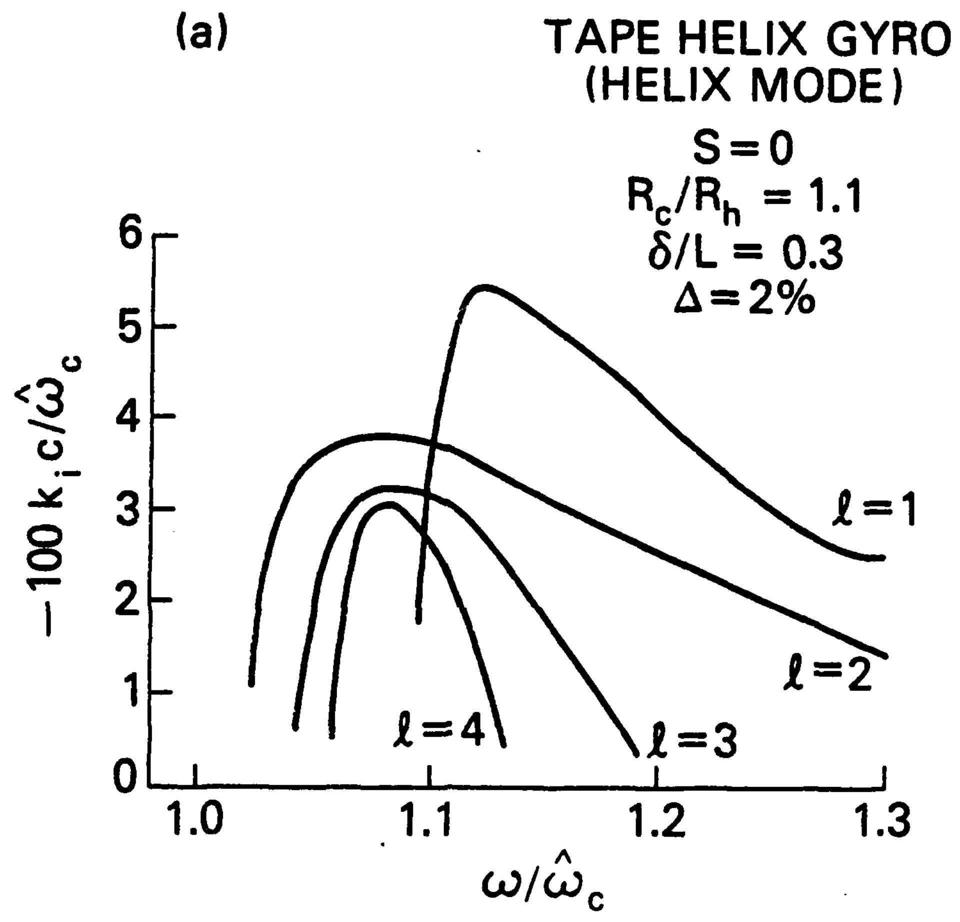

FIGURE 2. PLOTS OF THE NORMALIZED GROWTH RATE $k_i c/\hat{\omega}_c$ VERSUS $\omega/\hat{\omega}_c$ OBTAINED FROM EQUATION (39) FOR THE HELIX MODE, R_c/R_h = 1.1, $R_0 = R_h - r_L$, $s = 0$, $\delta/L = 0.3$, (a) $\Delta = 0.02$, (b) $\Delta = 0.04$, AND OPTIMUM VALUES OF THE PARAMETERS ($R_h\omega_c/c$, ϕ) GIVEN BY (1.06, 10.7°) FOR ℓ = 1, (2.15, 11.4°) FOR ℓ = 2,(3.2, 11°) FOR ℓ = 3, AND (4.2, 10°) FOR ℓ = 4

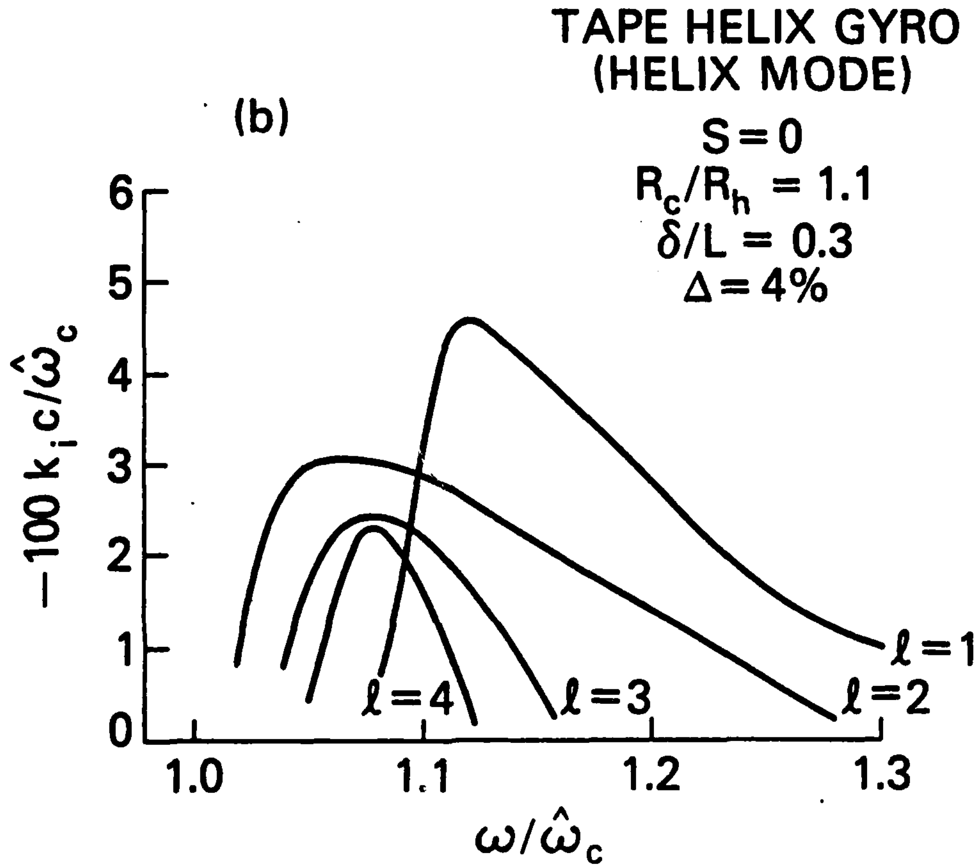

FIGURE 2. (CONTINUED)

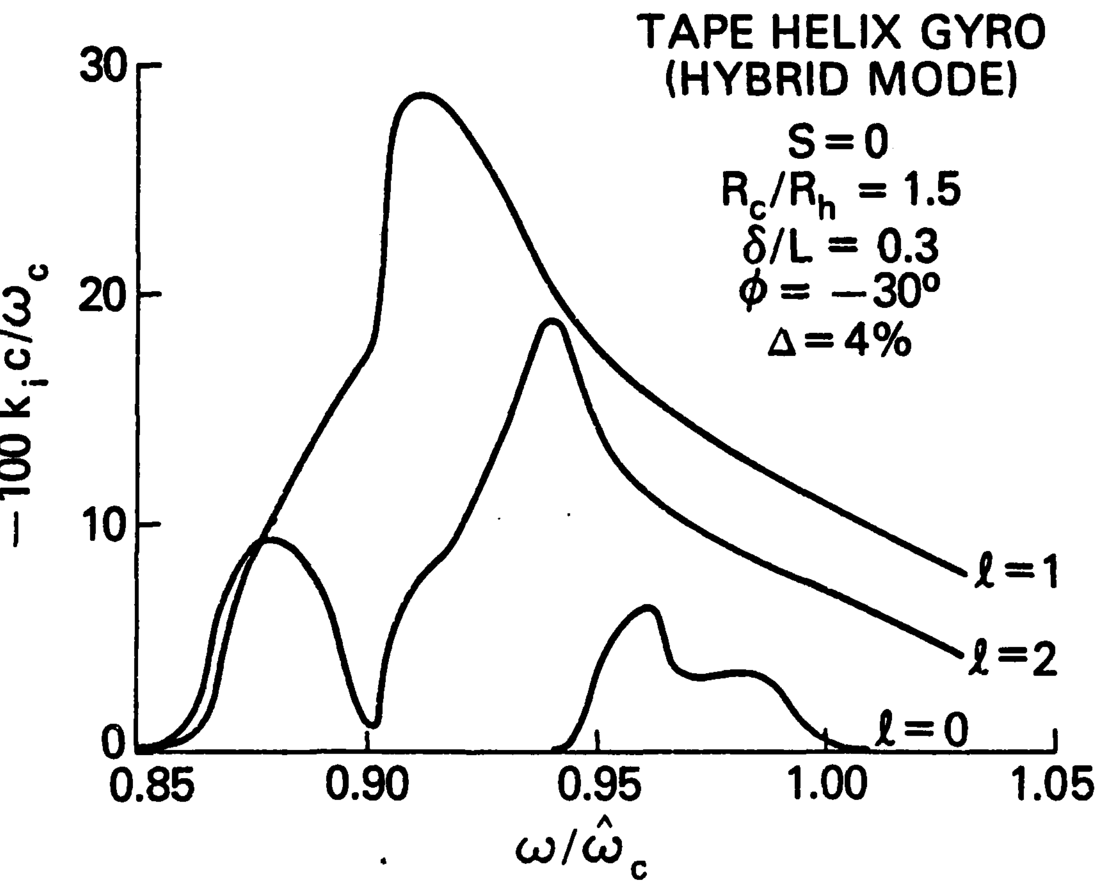

FIGURE 3. PLOTS OF THE NORMALIZED GAIN $k_i c/\hat{\omega}_c$ VERSUS $\omega/\hat{\omega}_c$ OBTAINED FROM EQUATIONS (39) AND (42) FOR $s = 0$, $R_c/R_h = 1.5$, $\delta/L = 0.3$, $\Delta = 0.04$, $R_0 = R_h - r_L$, $\phi = -30°$ AND $R_h\hat{\omega}_c/c = 1.86$ FOR $\ell = 0$, $R_h\hat{\omega}_c/c = 1.47$ FOR $\ell = 1$, $R_h\hat{\omega}_c/c = 2.4$ FOR $\ell = 2$

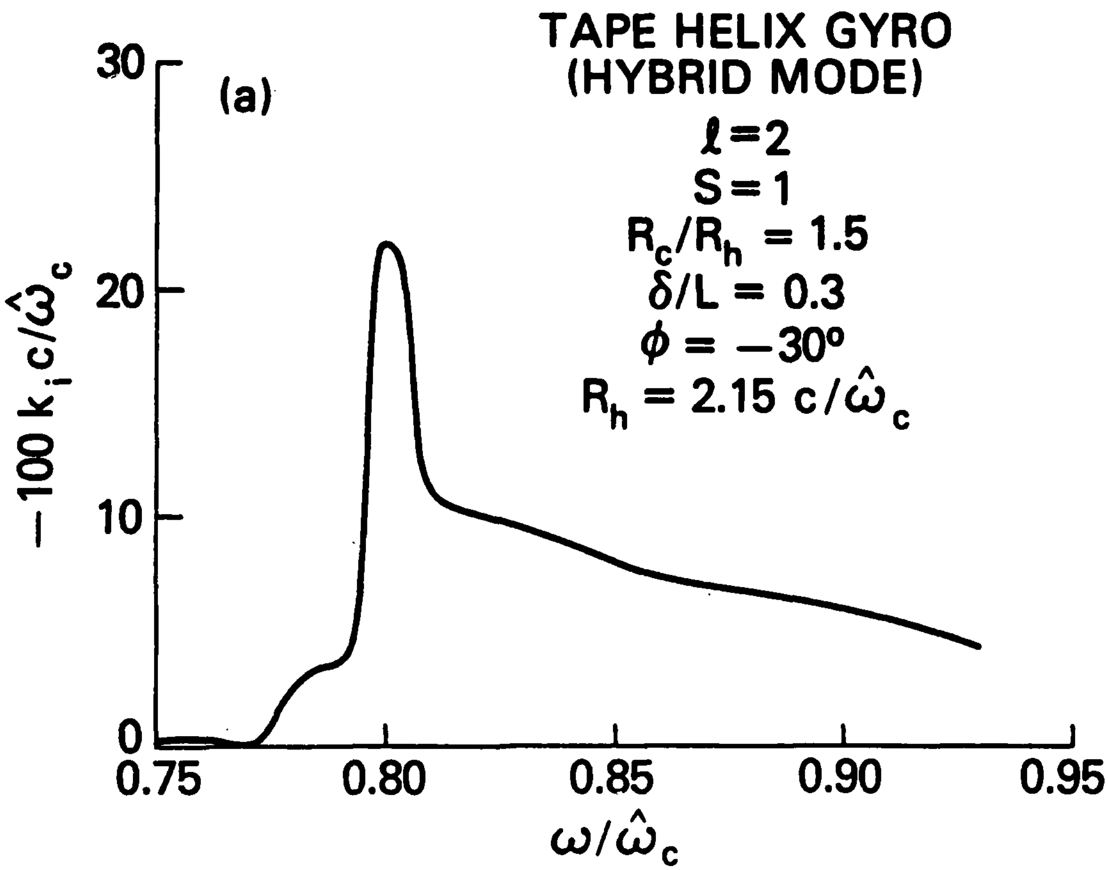

FIGURE 4. PLOTS OF THE NORMALIZED GROWTH RATE $k_i c/\hat{\omega}_c$ VERSUS $\omega/\hat{\omega}_c$ OBTAINED FROM EQUATIONS (39) AND (42) FOR $\ell = 2$, $R_c/R_h = 1.5$, $\delta/L = 0.3$, $\phi = -30^\circ$, AND (a) $R_h\hat{\omega}_c/c = 2.15$ FOR $s = 1$, (b) $R_h\hat{\omega}_c/c = 2.4$ FOR $s = 0$ AND (c) $R_h\hat{\omega}_c/c = 2.54$ FOR $s = -1$

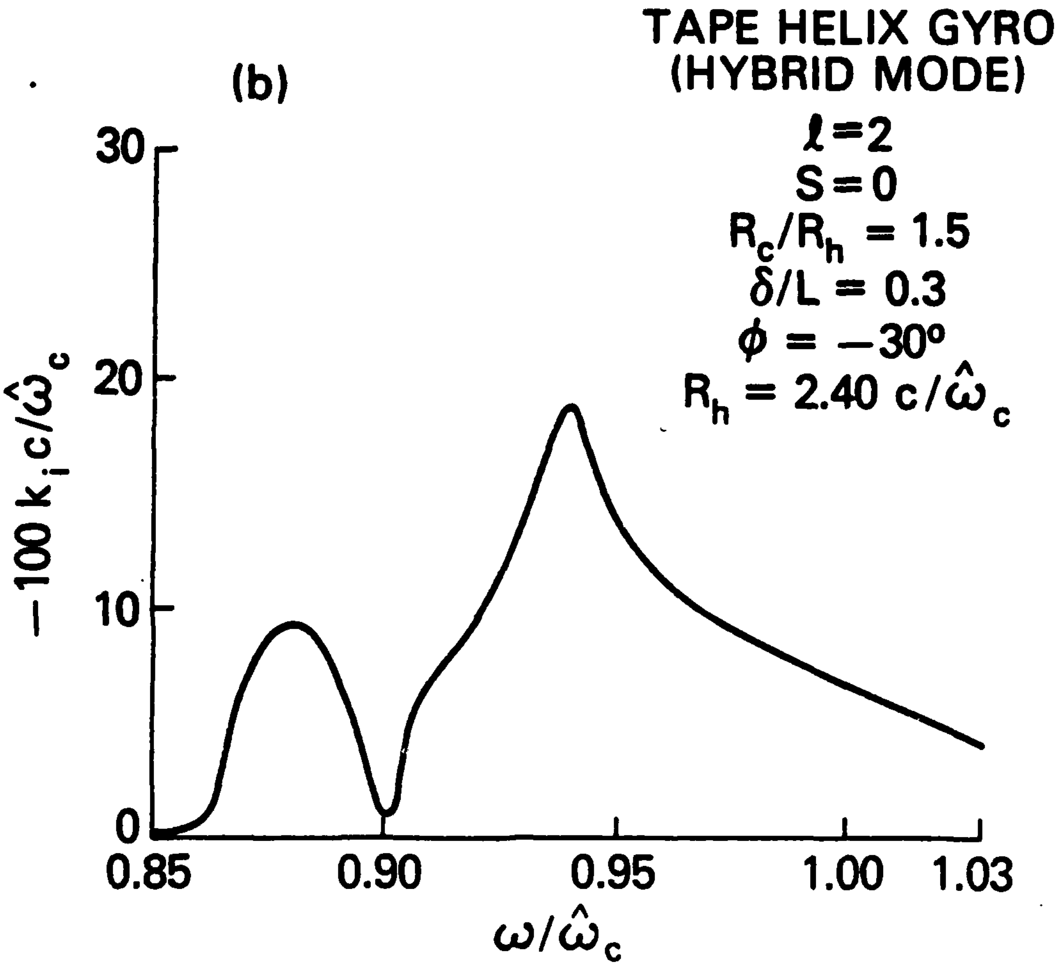

FIGURE 4. (CONTINUED)

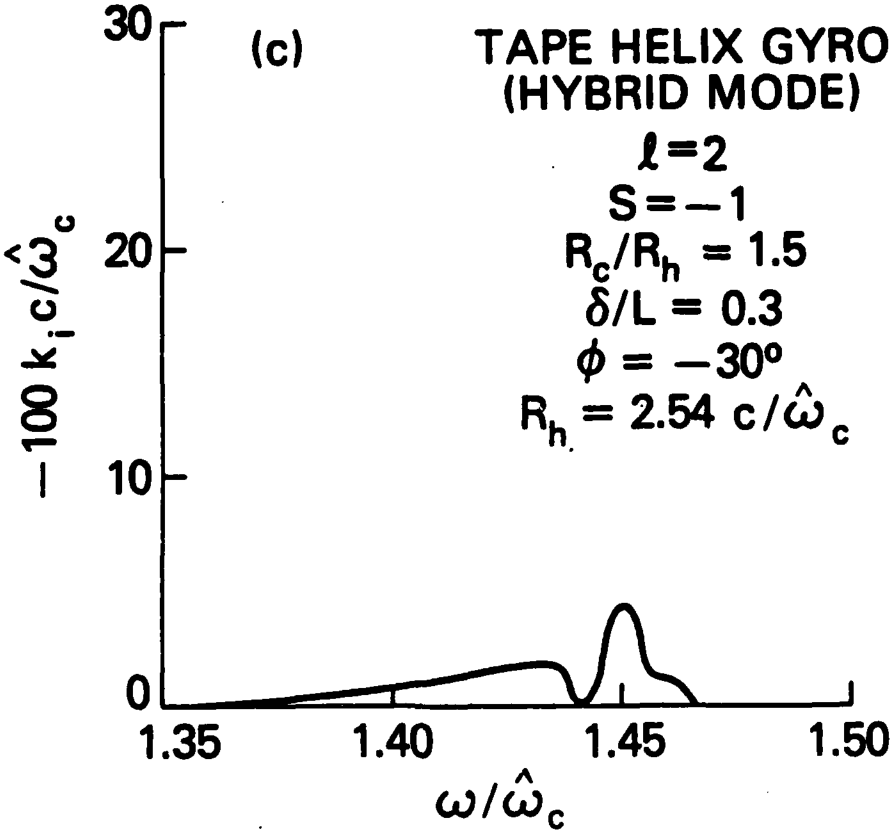

FIGURE 4. (CONTINUED)

REFERENCES

1. H. S. Uhm, R. C. Davidson and K. R. Chu, Phys. Fluids 21, 1877 (1978).

2. H. S. Uhm and R. C. Davidson, Phys. Fluids 23, 2538 (1980).

3. J. Y. Choe, H. S. Uhm and S. Ahn, J. Appl. Phys. 52, 7067 (1981), and the references therein.

4. K. R. Chu, Phys. Fluids 21, 2354 (1978).

5. H. S. Uhm and J. Y. Choe, "Gyrotron Amplifier in a Helix Loaded Waveguide," submitted for publication.

6. D. A. Watkins, Topics in Electromagnetic Theory (John Wiley, N.Y. 1958) Chapter 2.

7. H. S. Uhm and J. Y. Choe, "Electromagnetic Wave Propagation in a Tape Helix Waveguide," submitted for publication.

DISTRIBUTION

	Copies		Copies
Dr. Richard E. Aamodt Science Application Inc. 934 Pearl St. Suite A Boulder, CO 80302	1	Dr. J. Bayless DARPA Attn: DEO 1400 Wilson Blvd. Arlington, VA 22209	1
Dr. Saeyoung Ahn Code 5205 Naval Research Lab. Washington, D.C. 20375	1	Dr. Robert Behringer ONR 1030 E. Green Pasadena, CA 91106	1
Dr. Wahab A. Ali Naval Research Lab. Code 4700 4555 Overlook Ave., S.W. Washington, D.C. 20375	1	Prof. George Bekefi Bldg. 36-213, MIT 77 Massachusetts Ave. Cambridge, MA 02139	1
Dr. Donald Arnush TRW, Plasma Physics Dept. R1/107 1 Space Park Rodondo Beach, CA 90278	1	Dr. Gregory Benford Physics Department University of California Irvine, CA 92717	1
Dr. J.M. Baird Code 4740 (B-K Dynamics) Naval Research Lab. 4555 Overlook Ave., S.W. Washington, D.C. 20375	1	Dr. Jim Benford Physics International Co. 2700 Merced St. San Leandro, CA 94577	1
Dr. William A. Barletta Lawrence Livermore National Lab. L-321 University of California Livermore, CA 94550	1	Dr. Kenneth D. Bergeron Plasma Theory Div. - 5241 Sandia Laboratories Albuquerque, NM 87115	1
Dr. L. Barnett Code 4740 (B-K Dynamics) Naval Research Lab. 4555 Overlook Ave., S.W. Washington, D.C. 20375	1	Dr. T. Berlincourt Office of Naval Research Department of the Navy Arlington, VA 22217	1

DISTRIBUTION (Cont.)

	Copies
Dr. I. B. Bernstein Yale University Mason Laboratory 400 Temple Street New Haven, CT 06520	1
Dr. O. Book Code 4040 Naval Research Laboratory Washington, D.C. 20375	1
Dr. Jay Boris Naval Research Lab. Code 4040 4555 Overlook Ave., S.W. Washington, D.C. 20375	1
Dr. Howard E. Brandt Harry Diamond Labs 2800 Powder Mill Road Adelph, MD 20783	1
Dr. R. Briggs Lawrence Livermore Lab. P.O. Box 808 Livermore, CA 94550	1
Dr. K. Brueckner La Jolla Institute P.O. Box 1434 La Jolla, CA 92038	1
Dr. Herbert L. Buchanan Lawrence Livermore National Lab L-321 University of California Livermore, CA 94550	1
Dr. K. J. Button Massachusetts Institute of Technology Francis Bitter National Magnet Laboratory Cambridge, MA 02139	1

	Copies
Dr. Neal Carron Mission Research Corp. 735 State Street Santa Barbara, CA 93102	1
Dr. Frank Chambers Lawrence Livermore National Lab. L-321 University of California Livermore, CA 94550	1
Prof. F. Chen Dept. of E. E. UCLA Los Angeles, CA 90024	1
Dr. M. Caponi TRW Advance Tech. Lab. 1 Space Park Redondo Beach, CA 90278	1
Dr. K. R. Chu Naval Research Lab. Code 4740 4555 Overlook Ave., S.W. Washington, D.C. 20375	1
Dr. Timothy Coffey Naval Research Lab. 4555 Overlook Ave., S.W. Washington, D.C. 20375	1
Dr. W. J. Condell Office of Naval Research Code 421 Department of the Navy Arlington, VA 22217	1
Dr. G. Cooperstein Naval Research Lab. Washington, D.C. 20375	1
Dr. Edward Cornet W.J. Schafer Associates, Inc. 1901 North Fort Myer Dr. Arlington, VA 22209	1

DISTRIBUTION (Cont.)

	Copies
Prof. R. Davidson Plasma Fusion Center Massachusetts Inst. of Technology Cambridge, MA 02139	1
Dr. J. Dawson Dept. of Physics UCLA Los Angeles, CA 90024	1
Dr. W. Destlar Dept. of Electrical Engineering University of Maryland College Park, MD 20742	1
Prof. P. Diament Columbia University Dept. of Electrical Engineering New York, NY 10027	1
Prof. W. Doggett NC State University P.O. Box 5342 Raleigh, NC 27650	1
Dr. H. Dreicer Plasma Physics Division Los Alamos Scientific Lab. Los Alamos, NM 87544	1
Dr. A. Drobot Naval Research Laboratory Code 4790 (SAI) Washington, D.C. 30275	1
Prof. W. E. Drummond Austin Research Associates 1901 Rutland Drive Austin, TX 78758	1
Prof. H. H. Fleischmann Lab. for Plasma Studies and School of Applied and Engr. Physics Cornell University Ithaca, NY 14850	1

	Copies
Dr. D. Eccleshall U.S. Army Ballistic Research Lab. Aberdeen Proving Ground, MD 21005	1
Dr. Barbara Epstein Sandia Laboratories Albuquerque, NM 87185	1
Dr. A. Fisher Physics Dept. University of California Irvine, CA 92664	1
Dr. R. J. Faehl Los Alamos Scientific Lab. Los Alamos, NM 87544	1
Dr. Leon Feinstein Science Applications, Inc. 5 Palo Alto Square Palo Alto, CA 94304	1
Dr. Franklin Felber Western Research Corporation 8616 Commerce Ave. San Diego, CA 92121	1
Dr. Richard Fernslor Code 4770 Naval Research Lab. 4555 Overlook Ave., S.W. Washington, D.C. 20375	1
Dr. Thomas Fessenden Lawrence Livermore National Lab. L-321 University of California Livermore, CA 94550	1

DISTRIBUTION (Cont.)

	Copies
Dr. Robert Fossum, Director DARPA 1400 Wilson Boulevard Arlington, VA 22209	1
Dr. H. Freund Naval Research Lab. Code 4790 4555 Overlook Ave., S.W. Washington, D.C. 20375	1
Dr. M. Friedman Code 4700.1 Naval Research Laboratory Washington, D.C. 20375	1
Dr. B. Godfrey Mission Res. Corp. 1400 San Mateo Blvd, S.E. Suite A Albuquerque, NM 87108	1
Dr. T. Godlove Office of Inertial Fusion U.S. Department of Energy Washington, D.C. 20545	1
Dr. Jeffry Golden Naval Research Laboratory Washington, D.C. 20375	1
Dr. S. Goldstein Jaycor (Code 4770) Naval Research Lab. Washington, D.C. 20375	1
Dr. Victor Granatstein Naval Research Lab. Washington, D.C. 20375	1
Dr. S. Graybill Harry Diamond Lab. 2800 Powder Mill Rd. Adelphi, MD 20783	1
Dr. Michael Greenspan McDonnell Douglas Corp. St. Louis, MO 63166	1

	Copies
Dr. Robert Greig Naval Research Lab. (Code 4763) 4555 Overlook Ave., S.W. Washington, D.C. 20375	1
Dr. J.U. Guillory Jaycor 20050 Whiting St. Suite 500 Alexandria, VA 22304	1
Dr. Irving Haber Code 4790 Naval Research Lab. Washington, D.C. 20375	1
Prof. D. Hammer Lab. of Plasma Studies Cornell University Ithaca, NY 14850	1
Dr. Robert Hill Physics Division. #341 National Science Foundation Washington, D.C. 20550	1
Dr. J. L. Hirshfield Yale University Mason Laboratory 400 Temple Street New Haven, CT 06520	1
Dr. Richard Hubbard Code 4790 (Jaycor) Naval Research Lab. 4555 Overlook Ave., S.W. Washington, D.C. 20375	1
Dr. Bertram Hui Naval Research Lab. Code 4790 4555 Overlook Ave., S.W. Washington, D.C. 20375	1
Dr. S. Humphries Sandia Laboratories Albuquerque, NM 87115	1

DISTRIBUTION (Cont.)

	Copies
Dr. Robert Johnston Science Applications, Inc. 5 Palo Alto Square Palo Alto, CA 94304	1
Dr. Howard Jory Varian Associates, Bldg. 1 611 Hansen Way Palo Alto, CA 94303	1
Dr. Glenn Joyce Code 4790 Naval Research Lab. 4555 Overlook Ave., S.W Washington, D.C. 20375	1
Dr. Selig Kainer Naval Research Lab. 4555 Overlook Ave., S.W. Washington, D.C. 20375	1
Dr. C.A. Kapetanakos Plasma Physics Division Naval Research Laboratory Washington, D.C. 20375	1
Dr. Denis Keefe Lawrence Beskeley Lab. 1 Cyclotron Road Berkeley, CA 94720	1
Dr. Douglas Keeley Science Applications, Inc. 5 Palo Alto Square Palo Alto, CA 94304	1
Dr. Hogil Kim A & FR Div. Lawrence Berkeley Lab. Berkeley, CA 94720	1
Dr. Hong Chul Kim A & FR Div. Lawrence Berkeley Lab. Berkeley, CA 94720	1

	Copies
Dr. Kwang Je Kim Bldg. 64 #223 A & FR Div. Lawrence Berkeley Lab. Berkeley, CA 94720	1
Dr. Jin Joong Kim North Carolina State University Raleigh, NC 27607	1
Prof. N. M. Kroll La Jolla Institutes P.O. Box 1434 La Jolla, CA 92038	1
Dr. M. Lampe Naval Research Lab. Code 4790 4555 Overlook Ave., S.W. Washington, D.C. 20375	1
Dr. L. J. Laslett Lawrence Berkeley Lab. 1 Cyclotron Road Berkeley, CA 96720	1
Dr. Y. Y. Lau Naval Research Lab. Code 4740 (SAI) 4555 Overlook Ave., S.W. Washington, D.C. 20375	1
Dr. Glen R. Lambertson Lawrence Berkeley Lab. 1 Cyclotron Road, Bldg. 47 Berkeley, CA 94720	1
Dr. J. Carl Leader McDonnell Douglas Corp. Box 516 St. Louis, MO 63166	1

DISTRIBUTION (Cont.)

	Copies
Dr. W. M. Manheimer Naval Research Lab. Code 4790 4555 Overlook Ave., S. W. Washington, D. C. 20375	1
Dr. Edward P. Lee Lawrence Livermore National Lab L-321 University of California Livermore, CA 94550	1
Dr. Ray Lemke Air Force Weapons Lab Kirtland Air Force Base Albuquerque, NM 87117	1
Dr. Anthony T. Lin University of California Los Angeles, CA 90024	1
Dr. C. S. Liu Dept. of Physics University of Maryland College Park, MD 20742	1
Dr. Tom Lockner Sandia Laboratories Albuquerque, NM 87115	1
Dr. Conrad Longmire Mission Research Corp. 735 State Street Santa Barbara, CA 93102	1
Prof. R. V. Lovelace School of Applied and Eng. Physics Cornell University Ithaca, NY 14853	1
Dr. Joseph A. Mangano DARPA 1400 Wilson Blvd. Arlington, VA 22209	1

	Copies
Dr. James Mark L-477 Lawrence Livermore Lab Livermore, CA 94550	1
Dr. Jon A. Masamitsu Lawrence Livermore National Lab L-321 University of California Livermore, CA 94550	1
Dr. Bruce R. Miller Div. 5246 Sandia Laboratories Albuquerque, NM 87115	1
Dr. Melvin Month Department of Energy High Energy Physics Washington, D.C. 20545	1
Dr. Philip Morton Stanford Linear Accelerator Center P.O. Box 4349 Stanford, CA 94305	1
Dr. Don Murphy Naval Research Lab 4555 Overlook Ave., S.W. Washington, D.C. 20375	1
Dr. Won Namkung E. E. Department University of Maryland College Park, MD 20742	1
Prof. J. Nation Lab of Plasma Studies Cornell University Ithaca, NY 14850	1
Dr. V. Kelvin Neil Lawrence Livermore Nat'l Lab P.O. Box 808, L-321 Livermore, CA 94550	1

DISTRIBUTION (Cont.)

	Copies
Dr. Barry Newberger Mail Stop 608 Los Alamos National Lab Los Alamos, NM 87544	1
Dr. C. L. Olson Sandia Lab Albuquerque, NM 87115	1
Dr. Edward Ott Dept. of Physics University of Maryland College Park, MD 20742	1
Dr. Peter Palmadesso Bldg A50 #107 Naval Research Lab Washington, D.C. 20375	1
Dr. Ron Parkinson Science Applications, Inc. 1200 Prospect St. P.O. Box 2351 La Jolla, CA 92038	1
Dr. Richard Patrick AVCO - Everett Research Lab, Inc. 2385 Revere Beach Pkwy Everett, MA 02149	1
Dr. Robert Pechacek Naval Research Lab Code 4763 4555 Overlook Ave., S.W. Washington, D.C. 20375	1
Dr. Sam Penner National Bureau of Standards Bldg. 245 Washington, D.C. 20234	1
Dr. Michael Picone Naval Research Lab 4555 Overlook Ave., S.W. Washington, D.C. 20375	1

	Copies
Dr. R. Post Lawrence Livermore Lab University of California P.O. Box 808 Livermore, CA 94550	1
Dr. D. S. Prono Lawrence Livermore Lab P.O. Box 808 Livermore, CA 94550	1
Dr. S. Putnam Physics Internal Co. 2700 Merced St. San Leandro, CA 94577	1
Dr. Sid Putnam Pulse Sciences, Inc. 1615 Broadway, Suite 610 Oakland, CA 94612	1
Dr. Michael Raleigh Naval Research Lab Code 4763 4555 Overlook Ave., S.W. Washington, D.C. 20375	1
Dr. M. E. Read Naval Research Lab Code 4740 4555 Overlook Ave., S.W. Washington, D.C. 20375	1
Prof. M. Reiser Dept. of Physics & Astronomy University of Maryland College Park, MD 20742	1
Dr. M. E. Rensink Lawrence Livermore Lab P.O. Box 808 Livermore, CA 94550	1
Dr. Moon-Jhong Rhee E. E. Department University of Maryland College Park, MD 20742	1

DISTRIBUTION (Cont.)

	Copies
Dr. C. W. Roberson Naval Research Lab Code 4740 4555 Overlook Ave., S.W. Washington, D.C. 20375	1
Dr. J. A. Rome Oak Ridge National Lab Oak Ridge, TN 37850	1
Dr. Marshall N. Rosenbluth University of Texas at Austin Inst. for Fusion Studies RLM 11.218 Austin, TX 78712	1
Prof. Norman Rostoker Dept. of Physics University of California Irvine, CA 92664	1
Dr. C. F. Sharn Naval Sea Systems Command Department of the Navy Washington, D. C. 20363	1
Prof. S. P. Schlesinger Columbia University Dept. of Electrical Engineering New York, NY 10027	1
Prof. George Schmidt Physics Dept. Stevens Institute of Technology Hoboken, NJ 07030	1
Dr. Andrew M. Sessler Lawrence Berkeley Lab Berkeley, CA 94720	1
Dr. J. D. Sethian Naval Research Lab Code 4762 Washington, D.C. 20375	1
Dr. William Sharp Naval Research Lab Code 4790 (SAI) 4555 Overlook Ave., S.W. Washington, D.C. 20375	1
Dr. D. Straw AFWL Kirtland AFB, NM 87117	1
Dr. John Siambis Science Applications, Inc. 5 Palo Alto Square Palo Alto, CA 94304	1
Dr. J. S. Silverstein Code 4740 (HDL) Naval Research Lab 4555 Overlook Ave., S.W. Washington, D.C. 20375	1
Dr. M. Lee Sloan Austin Research Associates, Inc. 1901 Rutland Drive Austin, Texas 78758	1
Dr. L. Smith Lawrence Berkeley Lab 1 Cyclotron Road Berkeley, CA 94770	1
Dr. Joel A. Snow Senior Technical Advisor Office of Energy Research U.S. Department of Energy, M.S. E084 Washington, D.C. 20585	1
Dr. Philip Sprangle Naval Research Lab Code 4790 4555 Overlook Ave., S.W. Washington, D.C. 20375	1

DISTRIBUTION (Cont.)

	Copies
Dr. Doug Strickland Naval Research Lab Code 4790 (Beers) 4555 Overlook Ave., S W. Washington, D.C. 20375	1
Dr. Charles D. Striffler E. E. Dept. Univ. of Maryland College Park, MD 20742	1
Prof. R. Sudan Lab of Plasma Studies Cornell University Ithaca, NY 14850	1
Dr. C. M. Tang Naval Research Lab Code 4790 4555 Overlook Ave., S.W. Washington, D.C. 20375	1
Dr. R. Temkin Plasma Fusion Center Massachusetts Institute of Technology Cambridge, MA 02139	1
Dr. Lester E. Thode Mail Stop 608 Los Alamos National Lab Los Alamos, NM 87544	1
Dr. James R. Thompson Austin Research Associate, Inc. 1901 Rutland Drive Austin, Texas 78758	1
Dr. D. Tidman Jaycor 205 S. Whiting St. Alexandria, VA 22304	1
Dr. A. W. Trivelpiece Science Applications, Inc. San Diego, CA 92123	1

	Copies
Dr. John E. Walsh Department of Physics Dartmouth College Hanover, NH 03755	1
Dr. Wasneski Naval Air Systems Command Department of the Navy Washington, D.C. 20350	1
Dr. N. R. Vanderplaats Naval Research Laboratory Code 6805 4555 Overlook Ave., S. W. Washington, D.C. 20375	1
Lt. Col. W. Whitaker Defense Advanced Research Projects Agency 1400 Wilson Boulevard Arlington, VA 22209	1
Dr. Mark Wilson National Bureau of Standards Gaithersburg, MD 20760	1
Dr. Gerold Yonas Sandia Lab Albuquerque, NM 87115	1
Dr. Simon S. Yu Lawrence Livermore National Lab L-321 University of California Livermore, CA 94550	1
Defense Technical Information Center Cameron Station Alexandria, VA 22314	12

Internal distribution:

R	1
R04	1
R40	1

DISTRIBUTION (Cont.)

	Copies
Internal Distribution (Cont.)	
R401	1
R43 (C. W. Lufcy)	1
R44 (T. F. Zien)	1
R45 (H. R. Riedl)	1
R13 (J. Forbes)	1
R41 (P. O. Hesse)	1
R41 (R. Cawley)	1
R41 (M. H. Cha)	1
R41 (H. C. Chen)	1
R41 (J. Y. Choe)	1
R41 (R. Fiorito)	1
R41 (O. F. Goktepe)	1
R41 (M. J. Rhee)	1
R41 (D. W. Rule)	1
R41 (Y. C. Song)	1
R41 (H. S. Uhm)	1
R43 (A. D. Krall)	1
F	1
F14 (H. C. Coward)	1
F40 (J. F. Cavanagh)	1
F10 (K. C. Baile)	1
F46 (D. G. Kirkpatrick)	1
F34 (R. A. Smith)	1
F34 (E. Nolting)	1
F34 (V. L. Kenyon)	1
F04 (M. F. Rose)	1
F34 (F. Sazama)	1
N14 (R. Biegalski)	1
E431	9
E432	3
E35	1

4 -

DT